General Disclaimer

One or more of the Following Statements may affect this Document

- This document has been reproduced from the best copy furnished by the organizational source. It is being released in the interest of making available as much information as possible.

- This document may contain data, which exceeds the sheet parameters. It was furnished in this condition by the organizational source and is the best copy available.

- This document may contain tone-on-tone or color graphs, charts and/or pictures, which have been reproduced in black and white.

- This document is paginated as submitted by the original source.

- Portions of this document are not fully legible due to the historical nature of some of the material. However, it is the best reproduction available from the original submission.

NASA Technical Memorandum 83798

Plasma Variables and Tribological Properties of Coatings in Low Pressure (0.1 - 10.0 torr) Plasma Systems

R. Avni and T. Spalvins
Lewis Research Center
Cleveland, Ohio

Prepared for the
Eleventh International Conference on Metallurgical Coatings
sponsored by the American Vacuum Society
San Diego, California, April 9-13, 1984

NASA

PLASMA VARIABLES AND TRIBOLOGICAL PROPERTIES OF COATINGS IN LOW PRESSURE (0.1 - 10.0 torr) PLASMA SYSTEMS

R. Avni* and T. Spalvins
National Aeronautics and Space Administration
Lewis Research Center
Cleveland, Ohio 44135

SUMMARY

The interactions of plasma's particle fluxes such as positive ions, excited metastables and radicals (atoms and molecules) and radiation flux, with the substrate surface prior and during the deposition process is reviewed. The concept of plasma layer and the near-to-surface plasma region is introduced phenomenologically as the dialog between the plasma and the substrate surface.

Experimental evidence of the interactions between plasma and substrate such as: adsorption, morphological changes, defect formation, sputtering, chemical etching, and secondary electron emission is discussed as promoting and enhancing the surface chemistry, thus influencing the tribological properties of the deposited flux. Phenomenological correlations of rate of deposition, flux composition, microhardness and wear with the plasma layer variables give an insight to the formation of chemical bonding between the deposited flux and the substrate surface.

INTRODUCTION

A solid substrate immersed into an electrodeless plasma system is exposed to a number of processes according to the kinetic energy and the mass of free particles populating the discharge and hitting its surface. A continuous "dialog" takes place between plasma's energetic particles and the substrate surface prior and during the deposition of the coating films. The aim in this work is a detailed treatment of this "dialog" known as plasma-surface interactions (PSI) with respect to the coating process and its tribological behavior.

The behavior of the substrate in a plasma system is shown as a luminous region in figure 1(a) to (c). Under the same plasma (of propylene and argon mixtures) conditions on similar graphite substrate, the luminous region called here plasma layer (PL) shows the following qualitative features:

(i) The thickness of the PL is largest for the biased substrate at minus 100 V (fig. 1(c)) when compared to substrate floated (fig. 1(a)) or grounded (fig. 1(b)).

---

*Ben Gurion University of the Negev, Beer Sheva, Israel and NRC-NASA Research Associate.

(ii) The PL luminosity is higher than the luminosity in the plasma bulk (PB) indicating that in the near-to-surface region occurs an enhanced excitation or/and ionization process.

(iii) The PL wraps around the negatively biased (fig. 1(c)) and the grounded substrates (fig. 1(b)) while on the floated (fig. 1(a)) is formed only on the surface facing the direction of the gas flow.

The related PSI controlling film deposition and etching and its tribological qualities are schematically divided in four regions according to their phenomenological behavior, as shown in figure 2, namely:

1. The plasma bulk (PB) in which homogeneous reactions as excitation, ionization, dissociation of monomers and formation of polymerized species take place (refs. 1 to 7). The mechanisms and the kinetics of formation of ions, excited metastables and radicals (refs. 8 to 15) and their transport to the substrate surface are an important step in the understanding of the deposition phenomena. The energetic particle fluxes from the PB and its radiation impinging on the solid, exchange energy with the surface, neutralize and create in the substrate a distinct region of neutralization or the altered layer (AL) (refs. 16 to 18).

2. In the AL two main processes (refs. 16 to 18) occur as a result of the impact of PB's energetic particles and radiation with the surface, namely,

(i) energy transfer to the surface electrons resulting in the ejection of secondary electrons back into the PB and,

(ii) momentum transfer to the lattice by collisions with nuclei. The consequences of cascade collisions are among others: backscattering, sputtering of atoms into the PB, lattice damage, chemical potential gradients (segregation), and surface chemistry.

From the motion of electrons and atoms inside and outside the AL, two more regions may be identified; the substrate bulk (SB) and the plasma layers (PL).

3. The SB supplies the atoms by segregation to the AL mainly due to the chemical potential gradient ($\nabla\mu ch$).

4. The PL a very near-to-the surface-region in which sputtered and etched atoms and molecules and secondary electrons from AL interact with the particles populating the PL from one side while from the other side the new population of the PL interact with the Al.

Both PL and AL being the connections between PB and SB are discussed in detail with regard to their chemical-interactions-mechanisms and the influence on the tribological behavior of the deposited films.

REACTIONS IN THE AL AND PL

The schematics of the four regions and the respective particle fluxes are shown in figure 2. The PB electrons with concentration $N_{e_{PB}}$, average energy

$\bar{\varepsilon}_{e_{PB}}$ and distribution functions $f(\varepsilon_e)_{PB}$ reach first the substrate surface and force on it a negative potential with respect to the PB potential. Part of the electrons flux, $j_{e_{PB}}$ will be repelled by the negative potential. Positive ions with concentration $n_{i_{PB}}$ will reach the surface through a space charge region - the sheath - with a flux j_{i_S} imposed by the Bohm criteria (ref. 19) with energies $\geq Te_{PB}$ (the electrons temperature). In the sheath j_{i_S} gain acceleration by the high electric fields E_S and hit the substrate surface. The ions flux reaching the surface will be neutralized (ref. 18) and adsorbed in the AL. Hagstrum (ref. 16) has shown experimentally in figure 3 for He^+, Ne^+, and Ar^+ ions to neutralize with a probability higher than 0.99 on a tungsten surface. The amount of reflected ions (fig.3) is smaller than 0.01 from their incoming flux, j_{i_S}. Fluxes of excited neutrals i.e., excited metastable states, j_{m_S} and excited radicals, j_{R_S} (fig. 2) reach as well the surface releasing their energy in the AL after being partly trapped or adsorbed. The AL adsorbs the energy and the momentum of the incoming flux of excited energetic particles.

The Altered Layer (AL)

Hagstrum (refs. 16 and 17), Kaminsky (ref. 18), Behrish (ref. 20), Taglauer (ref. 21), and partly Winters (ref. 15) summarized the neutralization mechanisms of ions and excited particles on a solid surface as:

(i) Interactions with electrons in the conductance band resulting with de-excitation by an Auger process or/and a de-excitation by a resonance process, which yield the emission of secondary electrons (γ). The γ ejection is by a potential or/and a kinetic process. Figures 4(a) and (b) show the energy distribution function of the γ electrons by potential ejection and the γ yield by a kinetic ejection, respectively.

(ii) Interactions with the atom nuclei in the lattice by a momentum transfer i.e., nuclear or cascade collisions lead to the motion of lattice atoms. Taglauer (ref. 21) has shown that for projectile rows with energy higher than 100 eV the energy loss to the lattice in a binary collision is constant. The energy needed to overcome both the binding and the threshold energies of an atom in the lattice, such that sputtering of atoms from the surface lattice can take place at projectile energy below 100 eV. Under ion irradiation, atoms and electrons are cautiously removed from the surface leaving vacancies behind it. In the AL migration of atoms from SB reach the surface, due to a chemical potential, leaving the surface in a high mobile state (ref. 22).

Hart et al., (ref. 23) bombarded Cu contaminated Si surfaces with Ne^+ (20 keV) or Ar^+ (0.8 keV) and estimated the Cu sputtered atoms from a depth of about 10 nm; Kornelsen (ref. 24) measured penetration of heavy ions (0.25 - 16 keV range) in W as being above 5 nm while Winters (ref. 15) estimated the AL depth in a plasma system as being about 3 nm. Depending on the projectile mass, energy and angle of impact, the thickness of AL may vary between 3 to 10 nm conditioned as well by the surface conditions. In a plasma-deposition

system it can be stated the Al plays the important role in the chemical bonding between the surface and the first atomic layers of the deposited films. The chemical bonding which is in the range of several eV (ref. 2) results with a better adhesion (ref. 2) a higher resistance to wear (refs. 25 and 26), withstands mechanical stresses higher than 5.10^8 Nm^{-2} (ref. 2) and sometimes have lower friction coefficients (refs. 26 to 28). Enhanced surface chemistry is shown in figure 5(a) for ion nitriding of steels, in figure 5(b) for surface boridation of Ti and steels, and in figure 5(c) for surface plasma etching.

Szabo and Wilhelmi (ref. 28(a)) in figure 5(a) after plasma nitriding the steel samples in NH_3, exposed it to Ar^+ bombardment and beside Fe the sputtered particles (detected by SIMS) were $FeNH_2$ and $FeNH_3$. Their chemical bond was not destroyed by Ar^+ during the sputtering process. Raveh et al., (ref. 28(b)) in figure 5(b) plasma bonded Ti and steel samples. The boride compounds were crystallite-6 Ti_3B_4 and FeB + Fe_2B, respectively. The formation of these chemical compounds during plasma boridation is closely followed by the measured microhardness at higher VHN values corresponding at a higher rate of formation of either Ti_3B_4 or FeB. Coburn et al., (ref. 28(c)) show the almost linear correlation between the sputtering of dimers (metal oxide) and their bond energy. At higher bond energy higher sputter ratio of $MO^+/M^+ + MO^+$ was obtained.

Table 1 shows friction coefficient values for metal-ceramic and ceramic-ceramic pairs as obtained in plasma systems.

The coefficient of friction values as measured on a pin-on-disc tribotester (refs. 25 to 28) indicate for metal-ceramic couples a low coefficient of friction and even lower values were obtained in ceramic-ceramic couples deposited onto steel substrates (ref. 25). These values were related by Bunshah (ref. 25) to the values of volume wear loss, i.e., low coefficient of friction go hand in hand with low wear rate. For example (ref. 25) a volume wear loss below $1.0x10^{-5}$ mm^{-3} as obtained for TiC - TiN couples for a run distance of 500 m under a load of 0.4 kgf. For comparison, in the same test, Bunshah (ref. 25) reported for steel-steel couple coefficient of friction values between 0.4 - 0.65 and the corresponding volume wear loss was above $5x10^{-3}$ mm^{-3} i.e., several orders of magnitude higher. It is our belief that this tribological behavior is correlated to the AL chemistry as discussed is section 3.2.

The Plasma Layer (PL)

The fluxes of ions, j_{Is}, excited metastables (atoms and molecules), j_{ms}, radicals, j_{Rs}, and radiation j_{Rad} bombarding a surface generate secondary electrons, j_{Rs}, (γ_i, γ_m, and γ_R, respectively) sputtered atoms, j_{Sputt}, reflected neutrals (after being trapped in the surface), j_{Ref}, and etched molecules, j_{Etch}, as schematically shown in figure 2.

The yield of secondary electrons, (γ) from the impact of Ar^+ at 600 eV, for example, is $\gamma_i = a\ 10^{-2}$ ($a >, 10$) from a metallic surface (ref. 3) and $a < 10$ from a nonmetallic surface (ref. 3). The yield value γ_m from the impact of Ar excited metastables (11.55 eV) is about of the same order of magnitude as γ_i (ref. 18). The maximum of γ_i energy distribution

function from Ar^+ is below 10 eV as shown in figure 4(a). The γ electrons released from the surface are accelerated by the high electric field, E_s, in the sheath, towards the PB. The calculated average values (ref. 29) of E_s, the energy of positive ions, $\bar{\varepsilon}_{is}$ bombarding the surface and the energy of γ_i electrons, $\bar{\varepsilon}_{es}$ from a graphite surface in an inductive rf plasma are shown in figure 6. Due to E_s the high energy secondary electron beam (HEEB) with energy ε_{es}, anisotropic energy distribution function, $F_{es}(\varepsilon_{es})$, and flux j_{es} undergoes collision with particle populating the near to substrate plasma region. The HEEB electrons lost their energy in such collisions along Z, a distance from the solid's surface, until equalizes the average energy of the electrons in the PB. Along Z a boundary condition is formed between the PL and the PB, (ref. 29) i.e.,

$$\bar{\varepsilon}_{es(Z=\Delta L)} = \int_{Z=0}^{Z=\Delta L} E_{es}\, F_{es}\,(E_{es},\, E_{is},\, Z,\, P,\, W)\, d\varepsilon_{es} \rightarrow E_{e_{PB}} \qquad (1)$$

with ΔL the thickness of the PL, P, and W the total gas pressure in the plasma system and net input power, respectively. The excitation and ionization of the particles populating the PL by the HEEB's electrons can be compared to some processes produced by the interaction with PB electrons (refs. 29 and 30). The ionization rate, dn_i/dt is expressed as:

$$\frac{dn_i}{dt} = S\, j_{es}\, q_{es} \left(1 + \frac{a_i\, n^2\, k_i\, \Delta L}{j_{es}\, q_{es}}\right) \qquad (2)$$

where q_{es} is the efficiency of ionization by HEEB's electrons, S is the PL cross section, a_i the ionization degree by the PB electrons, n the concentration of particles in the plasma (for one ionization step $n_e = n_i = a_i n$), and k_i the rate coefficient of ionization by PB electrons. Figure 7 shows the ratio of $(dn_i/dt)_{PL}/(dn_i/dt)_{PB}$ being about two orders of magnitude higher for the interaction with HEEB's than with the PB electrons. The thickness values of the PL, ΔL, were evaluated theoretically (ref. 30) and measured by emission spectroscopy is shown in figure 8. The relative spectral intensity (emission) ratio for the same particle, I_{PL}/I_{PB}, in PL and PB is shown in figure 9; the contribution of HEEB electrons (in the PL) to particle excitation to a higher electronic quantum level is greater than the contribution of PB electrons for the same quantum level. As stated before the fluxes of ions, excited metastables and radicals, bombarding a surface enhance its chemistry. The ion enhanced surface chemistry is illustrated in figures 10(a) and (b) for plasma chemical etching of silicon and aluminum, respectively. Film deposition and chemical etching in the same plasma system are contradictory occurring processes. An example is shown in figures 11(a) to (c) for the deposition of microcrystalline Si films from a rf plasma of $SiCl_4 + H_2 + Ar$ on a graphite substrate (fig. 11(a)) the chlorine contamination of the deposited Si films (fig. 11(b)) and Si etching rate by Cl atoms under Ar^+ irradiation (fig. 11(c)). Another example of correlation between deposition and etching rates is shown in figure 12 for Si and SiO_2 in $CF_4 + H_2$ plasmas.

To estimate the amount of material sputtered, and chemically etched with the material deposited the following was performed: Grounded Si single

crystal was introduced in an argon induced microwave plasma at 100 W in pressure range from S 10^{-2} to 2.0 torr. Table II compares the sputtering, etching, and deposition fluxes (cm^{-2} 5^{-1}) and rates (nms^{-1}). Microwave plasmas of Ar, Ar + F_2 and Ar + Cl_2 were used for evaluating the sputtering and the etching from the grounded Si single crystal. For deposition, SiF_4, $SiCl_4$, and $SiCl_4$ + H_2 were added instead of F_2 and Cl_2, respectively. The dissociation of SiF_4, $SiCl_4$, and $SiCl_4$ + H_2 in the microwave plasma results with the formation of F_2, Cl_2, and HCl, respectively. Although about the same partial pressures and fluxes of F_2 and Cl_2 were obtained, the addition of SiF_4, $SiCl_4$, and $SiCl_4$ + H_2 to Ar microwave plasma, enhances the deposition of microcrystalline Si fluxes well above the sputtering and etching phenomena.

In the PL, as schematically shown in figure 2, clusters should be formed prior to nucleation and the deposition process. Direct evidence for cluster formation in the PL was not found. Nevertheless indirect evidence is supplied in table III which compares the ionization and polymerization degrees is the PB with the PL for a rf plasma of 16 vol C_3H_6 in Ar. Normalized to a given concentration of C_3H_6 monomers in the plasma, the ionization and polymerization ($\sum C > 3$) degrees are higher by 10^2 and 10 respectively, is the PL (at a distance of 0.1 cm from the substrate surface) than in the PB, as a result of the interactions with the HEEB's electrons charged particles. With long range dipole, moments attract and attach excited large polymer molecules, enhancing the formation of clusters (ref. 31) in the PL nearest to the substrate surface.

An example is shown in figure 13 where ion bombardment of Xe^+ or Ar^+ on clean Si surface sputter away silicon cluster ion and (Si_n^{p+}) with a distribution from 2 to 10 atoms in the cluster (ref. 31(a)).

SURFACE CHEMICAL REACTIONS AND TRIBOLOGICAL BEHAVIOR

Chemical Reactions Not in a Plasma Environment

Exposures of metallic surfaces, like Ni (refs. 32 to 34), Fe (ref. 32) Cu (ref. 35), Al (ref. 36) among others, to oxygen produce a well defined chemisorbed layer which changes into the oxide as the surface concentration of O_2 is increased. Dissociative chemisorption ($O_2 \rightarrow 2O$) produces a coverage of about 0.4 monolayers where the oxygen atoms sit is fourfold sites at a distance of 0.9 Å above the Ni plane (ref. 33). The chemisorption followed by an oxide nucleation stage causes the surface to reconstruct with the formation of a nickel oxide structure (refs. 33 and 34). The oxygen-nickel reaction becomes very slow after the formation of 2 to 3 layers of oxide.

Ammonia is used instead of N_2 molecule in nitriding stainless steels at temperatures about 500° C (ref. 37) merely because it is easier to dissociate NH_3 to NH_2 and NH radicals on the hot metal surfaces. Nitride layers as thick as several μm were formed during nitriding periods beyond 15 hr (ref. 37).

The probability for the dissociation of N_2^+ ions on a cold metal surface (Ni, W or Mo) reaches unity for N_2^+ kinetic energies around ~100 ev

(38.15) although the dissociation energy of the N_2 molecule to N atoms is only 9.6 eV. Figure 14(a) and (b) show the probability for dissociation and the chemisorption of N atoms forming a nitride layer of approximately 30 to 100 Å thick (ref. 15). Figure 16(a) shows the probability that N atoms from N_2^* would remain trapped in the metal surface was about 0.2, 1.0, 80 percent of the atoms from N_2^* dissociation were reflected back.

Another form of chemical reactions with metal surfaces is the etching phenomena. For example X_eF_2 which behaves like F atoms has been shown (ref. 13) to spontaneously etch at ambient temperature, Si, Ta, Mo, Ti, and W or other materials producing volatile fluorides. Fluorine molecules etch Si (ref. 13) while chlorine molecules etch Al (ref. 39) at sufficient pressure to obtain a good surface coverage (40°). Figure 15 shows the fluorination of Si as measured by a quartz crystal microbalance; first F_2 produces an adsorbed layer, following by the formation of unsaturated fluoride like SiF_2 (ref. 41) and finally SiF_4 desorbs from the surface.

Even for a pure metal the phenomena described above are highly complex and according to Dearnaley (ref. 42) and Bagus (ref. 43) depends more upon solid-state physical mechanism than on chemistry. It is influenced by mechanical stress, clustering, island formation, nucleation, motion of anions and cations, coulombic attractions and the presence of defects. Winters et al., (refs. 13 and 15) concluded from the high reactivity of nitrogen atoms compared to the nitrogen molecule that "radicals frequently chemisorb on surfaces which appear inert to the parent molecule."

Chemical Reaction in a Plasma

The reaction between the surface and a parent molecule or atom is mainly exothermic as shown in table IV for boron, nitrogen, and carbon on various metallic surfaces. In order to have the reaction proceed as a large activation energy is needed as shown in table V for Si and SiO_2. The need for activation energy is avoided by dissociating the parent molecule in the gas state, by producing excited radicals and positive ions. The plasma system supplies the dissociation, fragmentation, excitation, polymerization, and ionization of the parent monomer as shown in figures 16(a) and (b) for hydrocarbons and tetrachlorosilane, respectively. These excited radicals, atoms and positive ions react spontaneously (refs. 10 to 12) with the surface and probably produce the chemical bond necessary to the adhesion of the deposited film to the substrate surface, or interface (refs. 27 and 28).

Tribological Behavior of Refractory Coatings

To improve the frictional and wear properties of contacting surfaces it is customary in tribological practice to increase the surface and subsurface hardness. Hardened surfaces improve abrasive and adhesive wear resistance through the reduction of the real area of contact and by reducing the chemical activity between the materials at the rubbing interfaces. The fact remains that increasing the coating hardness of the flow strength of the coating increases and subsequently prevents deformation.

In recent years the plasma or low pressure glow discharge deposition techniques such as reactive sputtering and ion plating have emerged in various modes to supplement the well known case hardening, flame spraying, electroplating, PVD and CVD techniques. These ion assisted deposition techniques offer a great potential in tailoring the synthesis and deposition of refractory coatings for friction and wear control or both (refs. 28, and 44 to 51). Of the many refractory compounds nitrides and carbides are most widely investigated for tribological control (refs. 25, and 52 to 55).

During reactive sputtering or ion plating stable and metastable nitride and carbide compounds are formed by adjusting the partial pressure of the reactive gas such as N_2 or C_2H_2 respectively during the deposition. As a result, the change in stoichiometric composition of the respective compounds directly affects the hardness. Characteristic bulk and coating microhardness values reported in the literature are listed in table VI. Certainly, this large disparity in the hardness values is also reflected in the coefficient of friction as these coatings are tested in a pin-on-disc tribotester. Distinct differences in the coefficient of friction are reported depending whether both the steel disk and steel pin or only one of the tribo-components most likely the disk is coated. The high divergence in the coefficient of friction for steel/steel (0.45 - 0.55), ceramic coatings/steel (0.2 - 0.25), or ceramic coatings/ceramic coatings (0.08 - 0.18) systems are shown in figure 17.

At present TiN is by far the most widely investigated and used coating for tribological applications. A proposed phase diagram for titanium-nitrogen is shown in figure 18. The high variation in hardness values for TiN_X from 1500 to 4000 kg/mm^2 can be related to the stoichiometric composition. It is interesting to note that the variation in hardness can be related to the stoichiometric and mixed phase structure and this is also reflected in a distinct color change (from light to dark yellow). This relationship is shown in figure 19, where hardness and color are shown as a direct function of the atomic ratio x = N/Ti. The maximum hardness of 4000 kg/mm^2 exists over an atomic ratio (x) within the range of 0.55 to 0.7 and consists of a mixed phase structure. The stoichiometric TiN film where X = 1 exhibits a microhardness of about 2000 kg/mm^2 which corresponds very closely to the bulk value. No systematic correlation of the change in atomic ratio to the friction and wear characteristics has been reported.

The mode of wear and friction behavior of the nitride and carbide coatings is affected by their adherence and coherence. Adhesive loss results in flaking and cohesive failure of the coating results in chipping. Of the many parameters which determine the operation of the coating when external loads are applied as in tribo-contact, the residual stress consideration suggests that the $E\alpha$ product (E = Youngs Modulus, α = coefficient of thermal expansion) is a significant parameter in the choice of the coating/substrate system. Coatings possessing $E\alpha$ products that more closely match those of the substrate are the preferred ones, since lower flow/substrate interfacial shear stresses are induced during the frictional testing.

CONCLUSIONS

The understanding of film deposition processes in plasma systems is still in its infancy. The deposition "models" described have a phenomenologically

qualitative character. There is insufficient information on plasma surface interactions, chiefly due to the fact that few experiments have been done with known fluxes of radicals on well-defined surfaces and little is known about synergetic effects in plasma. The bondings to the surfaces (chemical, Van der Waals and electrostatic) which dominates the tribological behavior of the film are still poorly defined. It would be most desirable to perform well defined surface experiments inside a plasma system.

REFERENCES

1. J. A. Thornton; Thin Solid Films, 107, (1983), 3.

2. J. A. Thornton; Chaps. 2 and 5 in Deposition Technologies for Films and Coatings, R. F. Bunshah (Ed.), Noyes Pub., N. J., (1982).

3. B. N. Chapman; Glow Discharge Processes, J. Wiley, N. Y., (1980).

4. M. Shen, and A. T. Bell (Eds.); Plasma Polymerization, ACS Symp., Series 108, (1979).

5. A. T. Bell; Mechanism and Kinetics of Plasma Polymenization, Chap. in Topics in Current Chem. 94, Plasma Chem. III., S. Veprek and M. Venugopalan (Eds.), Springer Verlag, Berlin, (1980).

6. J. L. Vossen and J. J. Cuomo; Chap. II-1 in Thin Film Processes, J. L. Vossen and V. Kern (Eds.), Academic Press, N. Y., (1978).

7. Yasuda; Chap. IV-2 in Thin Film Processes, J. L. Vossen and V. Kern (Eds.), Academic Press, N. Y., (1978).

8. D. Smith; Plenary Lecture at the 6th ISPC Proc., Vol. 1, M. I. Boulos and R. J. Munz, (Eds.), Montreal, (1983).

9. G. Turban; Plenary Lecture at the 6th ISPC, Proc., Vol. 1, (as in 8).

10. N. Mayo, U. Carmi, I. Rosenthal, and R. Avni; to be published in J. Appl. Phys., (1984).

11. R. Avni, U. Carmi, I. Rosenthal, and A. Inspektor; 6th ISPC Proc., Vol. 2, p. 522, M. I. Boules and R. J. Munz (Eds.), Montreal, (1983).

12. R. Avni, U. Carmi, I. Rosenthal, R. Manory, and A. Grill; Thin Solid Films, 107, (1983), 235.

13. H. F. Winters, J. W. Coburn, and T. J. Chuang; J. Vac. Sci. Technol. B1, (1983), 469.

14. G. K. Vinogradov, P. I. Nevzorov, L. S. Polak, and D. I. Sloretsky; Vacuum, 32, (1982), 529.

15. H. F. Winters; Elementary Processes at Solid Surfaces Immersed in Low Pressure Plasmas, Chap. in Topics in Current Chem. 94, S. Veprek and M. Venugopalan (Eds.), Springer Verlag, Berlin, (1980).

16. H. D. Hagstrum; Phys. Rev. 123, (1961), 758.

17. H. D. Hagstrum; Low Energy De-Excitation and Neutralization Processes Near Surfaces in Inelastic Ion Surface Collisions, N. H. Tolk, J. C. Tully, W. Heiland, and C. W. White (Eds.), Academic Press, N. Y. (1977).

18. M. Kaminskii; Atomic and Ionic Impact Phenomena on Metal Surfaces Springer Velog, Berlin, (1965).

19. R. Behrish (Ed.); Sputtering by Ion Bombardment, Topic in Appl. Phys. Springer Velog, Berlin, (1980).

20. F. F. Chen; Chap. 3 in Plasma Diagnostics Techniques, R. H. Huddelstone and S. L. Leonard (Eds.), Academic Press, N. Y., (1965).

21. E. Taglauer and W. Heiland; Nucl. Instrm. Methods, 132, (1976), 535.

22. H. H. Andersen; Appl. Phys., 18, (1979), 131.

23. R. R. Hart, H. L. Dunlap, and J. O. Marsh; J. Appl. Phys., 46, (1975), 1947.

24. E. V. Kornelsen et al., Phys. Rev., 136, A, (1964), 849.

25. R. F. Bunshah; Thin Solid Films, 107, (1983), 21.

26. A. S. Korhonen, E. H. Sirvio and S. Sulonen; Thin Solid Films, 107, (1983), 387.

27. D. R. Wheeler and W. A. Brainard; Wear, 58, (1980), 341.

28. W. A. Brainard, NASA TP-1033, (1977).

29. Y. L. Khait, A. Inspektor, and R. Avni; Thin Solid Films, 72, (1980), 249.

30. Y. L. Khait, U. Carmi, and R. Avni; Proc. 6th ISPC, Vol. 2, p. 729, M. I. Boulos and R. J. Munz (Eds.), Montreal, (1983).

31. J. Lothe and G. M. Pound; The Replacement Factor in Nucleation Theory in Molecular Processes on Solid Surfaces, E. Dragulis, R. D. Gretz and R. I. Jaffee (Eds.), McGraw-Hill, N. Y., (1969).

32. C. R. Brundle in Aspects of the Kinetics and Dynamics of Surface Reactions, V.Z. Landman (Ed.), A.I.P., N.Y., (1980).

33. P. H. Holloway and J. B. Hudson; Surf. Sci., 43, (1974), 123.

34. D. F. Mitchell, P. B. Sewell, and M. Cohen; Surf. Sci., 61, (1976), 355.

35. P. T. Ling et al.; J. Vac. Sci. Technol., 21, (1982), 47.

36. T. W. Orent and S. D. Bader; Surf. Sci., 115, (1982), 323.

37. Metals Handbook Vol. 2, p. 149, 8th Edition American Society for Metals, Metals Park, Ohio, (1964).

38. H. F. Winters; J. Appl. Phys., 43, (1972), 4809.

39. D. L. Smith and R. H. Bruce; Extended Abstracts Electrochem. Soc., 81, 2, (1981), 258.

40. D. L. Smith; High Pressure Etching, Chapter to be published in Plasma Processing for VLSI, D. M. Brown (Ed.), Academic Press, (1984).

41. T. J. Chuang; J. Appl. Phys., 51, (1980), 2614.

42. G. Dearnaley; Nucl. Instrum. Methods, 182/183, (1981), 899.

43. P. S. Bagus, B. Liu, A. D. McLean, and M. Yoshimine in Computational Methods in Chemistry, J. Bargon (Ed.), p. 203, Plenum, N. Y., (1980).

TABLE I. - FRICTION COEFFICIENT DATA WITHOUT LUBRICATION AT LOW HUMIDITY ($\leq$50 PERCENT) IN PLASMA SYSTEMS

Material pair	Friction coefficient	Deposition method
Metal-ceramic		
304 - TiN	0.75	ARE (25)
304 - TiC	.42	ARE (25)
HSS - TiN	.18	Ion-Plated (26a)
440C-Mo_2B_5	.20	Sputtering (27)
440C-$MoSi_2$	.55	Sputtering (27)
Rene'41-TiC	.4	Sputtering (27)
440C-Mo_2C	.25	Sputtering (28)
440C-TiB_2	.2	Sputtering (28)
Ceramic-ceramic		
TiC - TiN	0.05-0.2	ARE (25)
TiN - TiN	0.65	ARE (25)
TiN-(Ti_2N-TiN)	0.1 -0.3	ARE (25)

TABLE II. - FLUXES AND RATES OF SPUTTERING, ETCHING AND DEPOSITION OF SILICON IN A MICROWAVE (2.45 GH_z) PLASMA:

[Kinetic energy of Ar^+ = 600eV. $N_1^{Ar+} = 10^{11} cm^{-3}$; $J_{Ar+} = 3.4\ 10^{16}\ cm^{-2}S^{-1}$; J_{F2} and J_{Cl2} about 10^{16} $cm^{-2}S^{-1}$; $5 10^{-2} \leq P \leq 2.0$ torr; Si substrate grounded.]

	Si					
	Sputter	Etch[a]		Deposition[b]		
Plasma	Ar	$Ar+F_2$	$Ar+Cl_2$	$Ar+SiF_4$	$Ar+SiCl_4$	$Ar+SiCl_4+H_2$
Flux $10^{16} cm^{-2}S^{-1}$	1.6	9.5	1.9	1.0	1.2	2.8
Rate nms^{-1}	---	0.08	0.03	0.2	0.22	1.55

[a]Fluxes calculated (refs. 13 and 15): Rates (refs. 14 and 15) on Si single crystal.

[b]5 vol % SiF_4 in Ar (unpublished)
5 vol % $SiCl_4$ in Ar (ref. 12) and,
5 vol % $SiCl_4$ + 15 vol % H_2 in Ar (ref. 12)
} deposit film microcrystalline Si at 0.5 and 2.9 torr

TABLE III. - IONIZATION AND POLYMERIZATION DEGREES IN A RF PROPYLENE - ARGON PLASMA IN PB AND PL.

[Graphite Substrate Grounded: $1 < P < 5$ torr.; 150 watt.]

	PB	PL
N_1/n^a	3×10^{-5}	5×10^{-3}
n Polym/n^a	2×10^{-5}	$>8 \times 10^{-1}$

[a]concentration of C_3H_6 in the gas mixture (16 vol % C_3H_6/Ar).

TABLE IV. - FREE ENERGY OF FORMATION AT 500° C Si

[Handbook of Refractory Compounds, G. V. Samsonov and I. M. Vinitskii IFI/Plenum NY (1980).]

Boriding		Nitriding		Carburizing	
$\Delta F_{773\ K}$ kcal.mole^{-1}					
$Ti+2B \rightarrow TiB_2$	-68.0	$Ti+1/2\ N_2 \rightarrow TiN$	-63.0	$Ti + C \rightarrow TiC$	-41.9
$2Ti+5B \rightarrow Ti_2B_5$	-99.5	$V + 1/2\ N_2 \rightarrow VN$	-43.5	$V + C \rightarrow VC$	-11.3
$V + 2B \rightarrow VB_2$	-60.0	$B+1/2\ N_2 \rightarrow 2Cr_2N$	-26.5	$7Cr+3C \rightarrow Cr_7C_3$	-46.4
$Cr+2B \rightarrow CrB_2$	-30.2	$B+1/2\ N_2 \rightarrow BN$	-18.5	$2Fe+C \rightarrow Fe_2C$	+2.0
		$Al+1/2N_2 \rightarrow BN$	-59.8	$4B+C \rightarrow B_4C$	-10.9
		$3Si+2N_2 \rightarrow Si_3N_4$	-117.8	$Si+C \rightarrow SiC$	-11.5

TABLE V. - ACTIVATION ENERGIES FOR SILICON AND SILICON DIOXIDE ETCHING BY FLUORINE IN A PLASMA SYSTEM

[G. K. Vinogradov et al. Vacuum 32, 529 (1982).]

Experimental conditions	Temperature range °C	Si etching activation energy	SiO_2 etching kcal mol^{-1}	Etch reaction probability at 25° C
p_F = 0.5 torr in plasma afterglow	300 - 600	---------	3.1 + 0.4	$2.4\ 10^{-5}$
CF_4+0.2 plasma	300 - 500	1.1 + 0.2	4.2 + 0.6	--------
CF_4+4 O_2 plasma p_F = 0.1 torr	300 - 550	2.7 + 0.4	2.3 + 0.3	--------
CF_4 plasma	300 - 500	3.1 + 0.4	4/2 + 0.5	--------
F_2 plasma in the afterglow	240 - 400	2.5 + 0.1	3.72	1.66×10^{-3} Si(F) 2.1×10^{-5} SiO_2(F)

TABLE VI. - MICROHARDNESS VALUES FOR NITRIDES AND CARBIDES

Material	Vickers Hardness kg/mm^2	
	Bulk	Films
TiN	2000	1500-4000
ZrN	1500	700-3600
HfN	1600	1850-2400
VN	1500	600-2000
NbN	1400	1100-3000
TaN	1000	---------
Si_3N_4	1000-2000	2000-3000
TiC	3500	2770-4150
VC	2500	1900-2850
WC	2050	1800-2800
TaC	2200	1280-2200

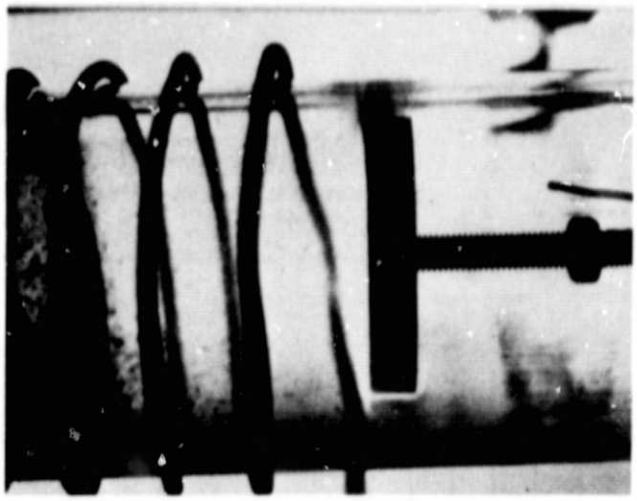

(a) Substrate floated.

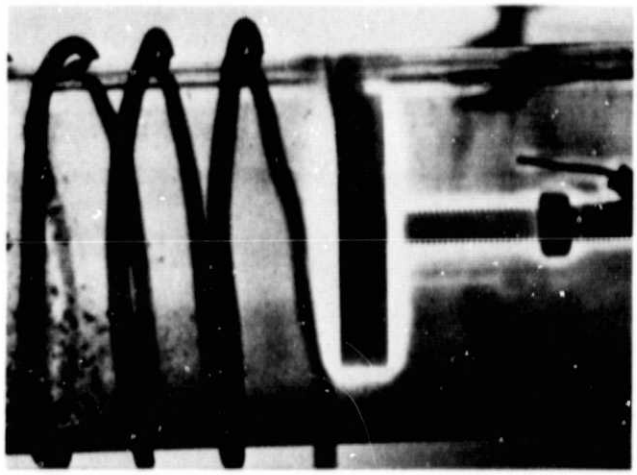

(b) Substrate grounded.

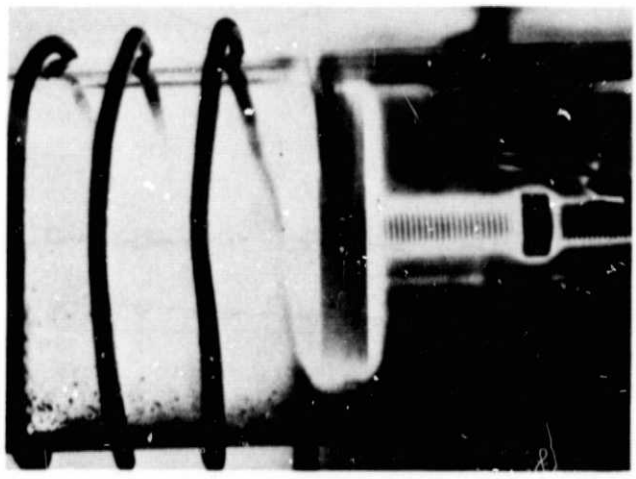

(c) Substrate biased at 100 volts.

Figure 1. - Luminous zone around a graphite substrate immersed in a RF plasma. (C_3H_6 + Ar at 500 watts power input).

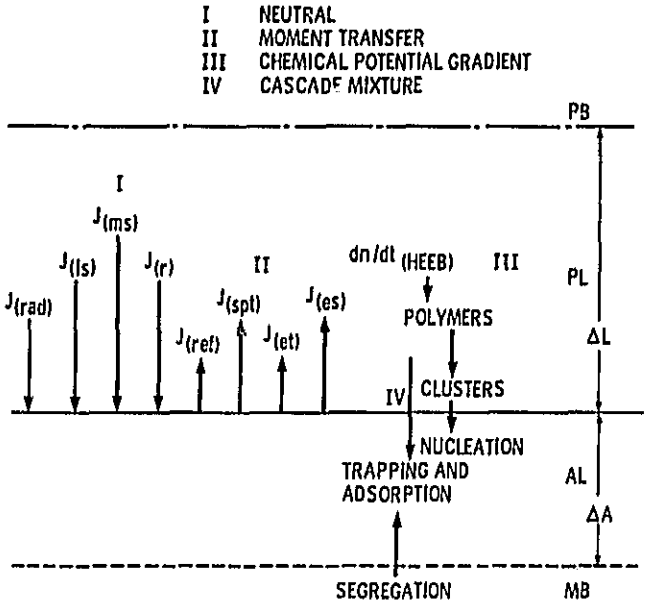

Figure 2. - Schematic representation of plasma surface interaction.

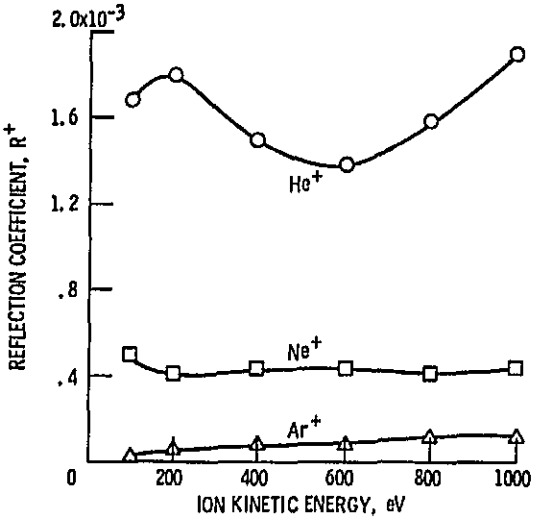

Figure 3. - Coefficient of reflection of rare-gas ions from a clean tungsten surface (ref. 16).

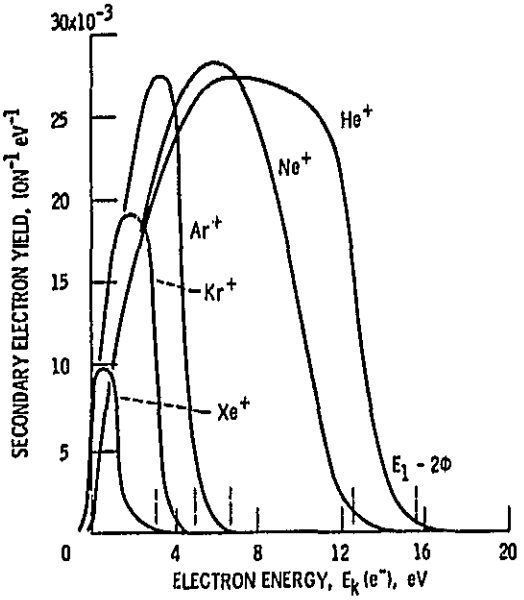

(a) Energy distribution function (potential ejection). Tungsten; 10-eV ions.

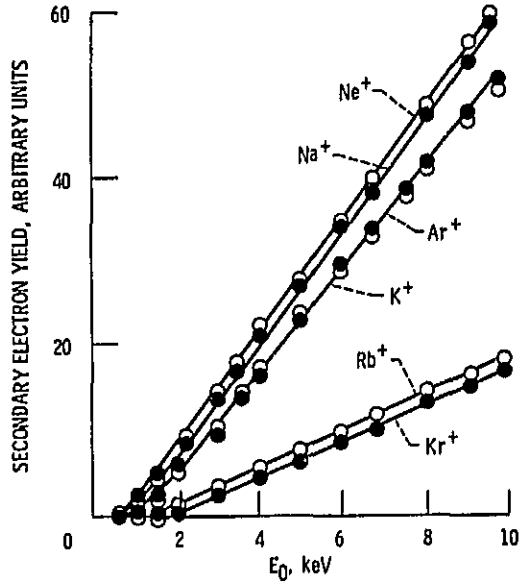

(b) γ Yield (kinetic ejection). Molybdenum.

Figure 4. - Secondary electrons ejected from a tungsten surface by rare gases and alkali ions.

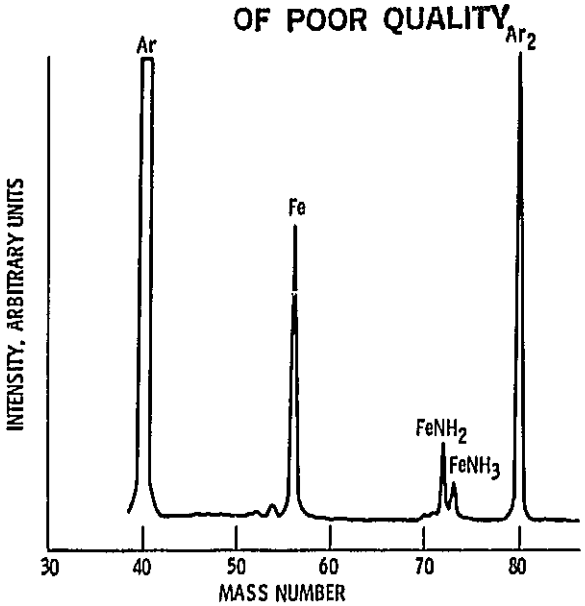

Figure 5. - Secondary ion mass spectrometry obtained for plasma nitriding of steels.

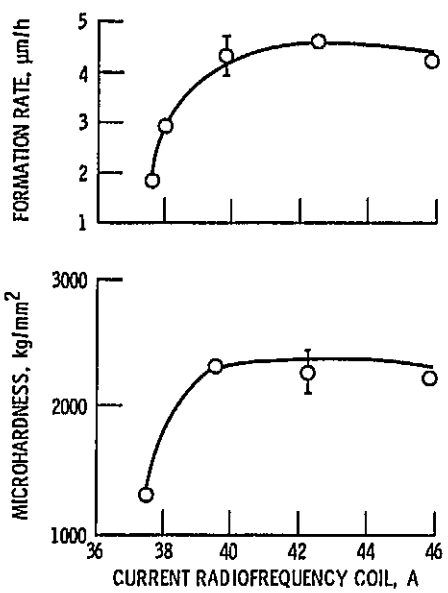

Figure 6. - Plasma boriding of stainless steel.

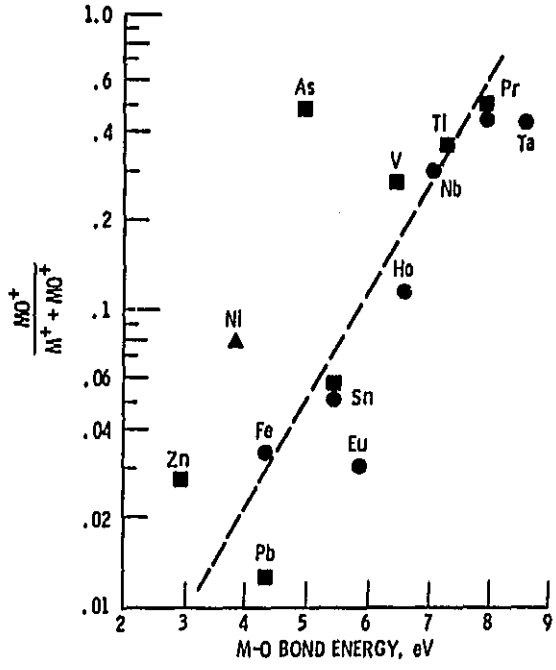

Figure 7. - Sputtering of dimers as a function of dimer bond energy. P_{Ar}, 60×10^{-3} torr; RF, 100 W (13.56 MHz).

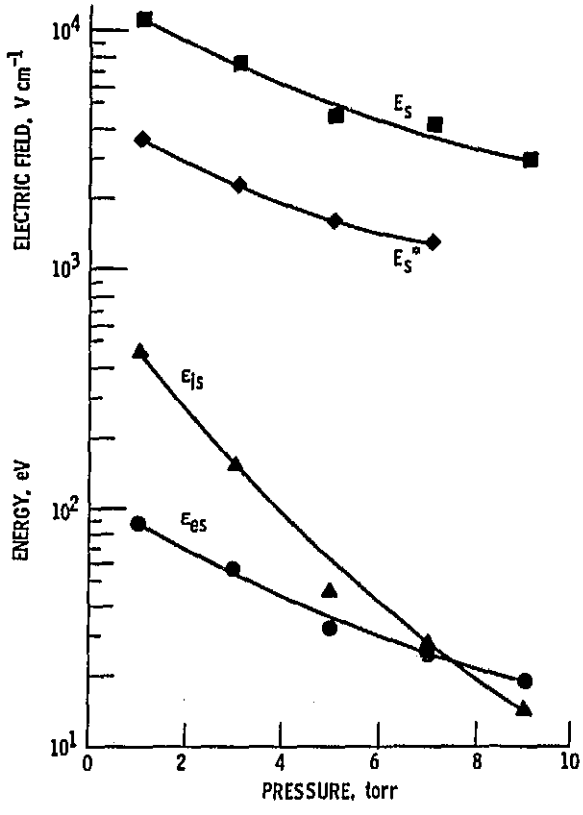

Figure 8. - Calculated values in sheath.

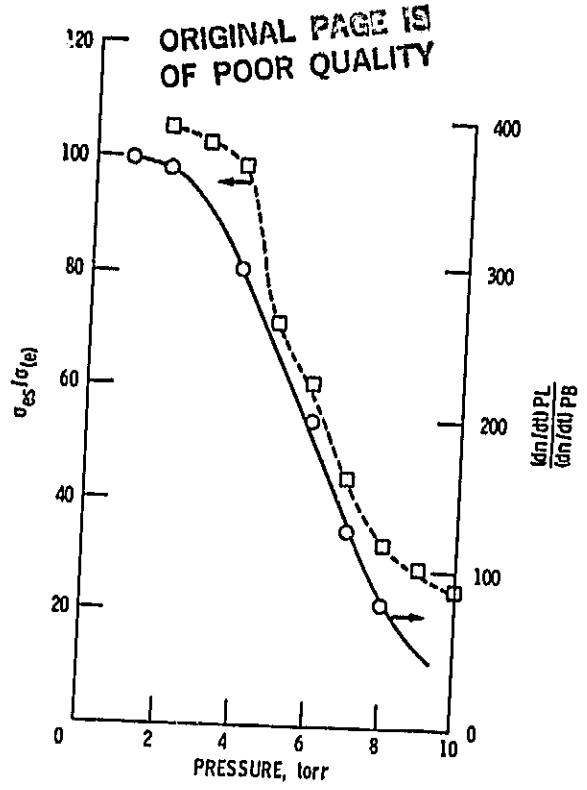

Figure 9. - Crosssection and ionization rate ratios in PL and PB.

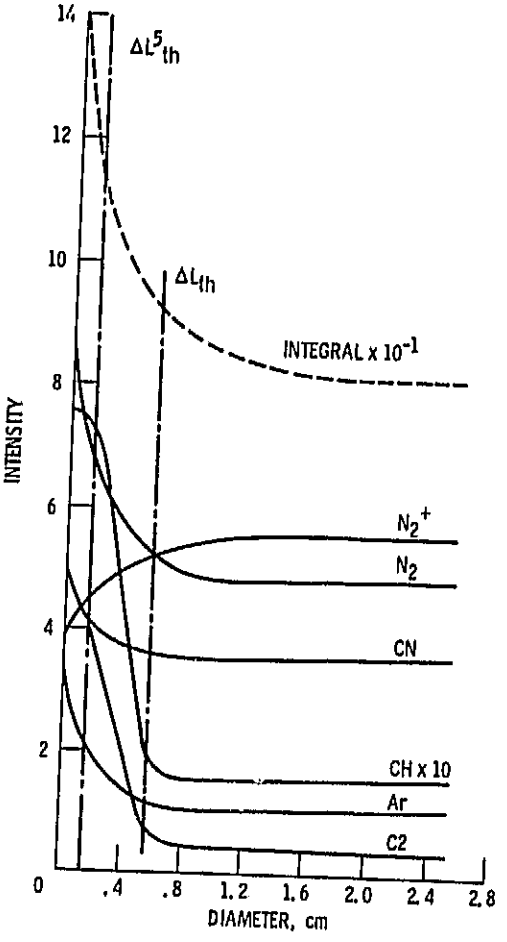

Figure 10. - Spectral intensity versus distance in the PL from surface. Pressure, 1.0 torr; power, 100 W.

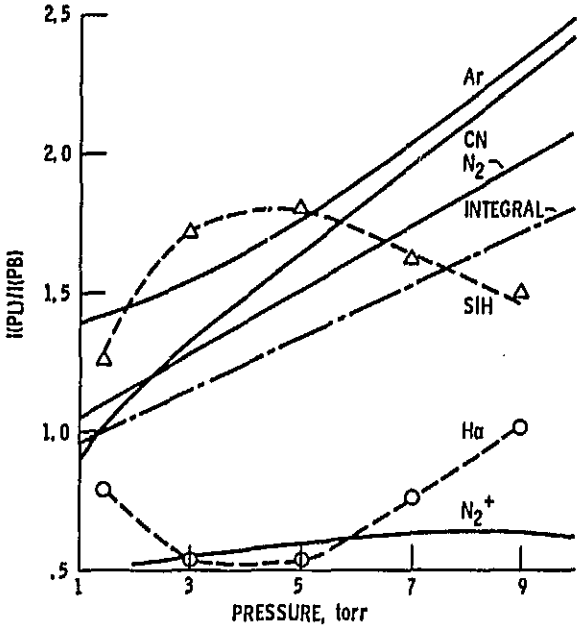

Figure 11. - Spectral intensity ratios versus gas pressure, Power, 100 W.

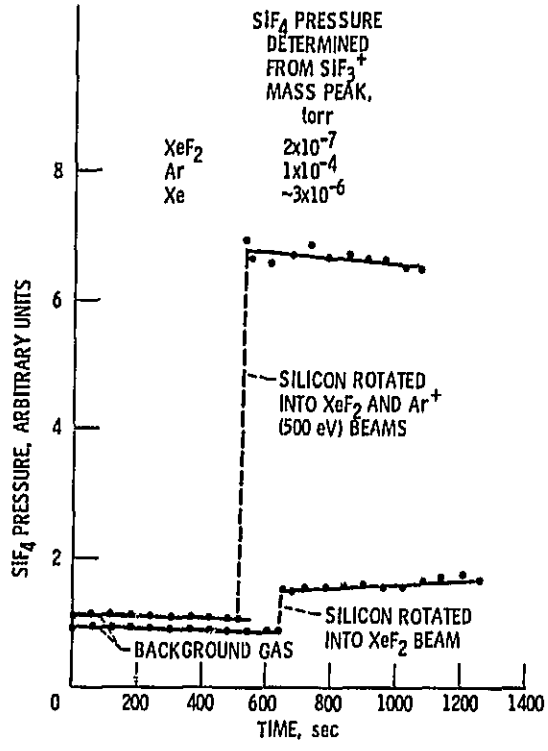

Figure 12. - Ion enhanced chemistry on silicon etching by $Ar^+ + XeF_2$.

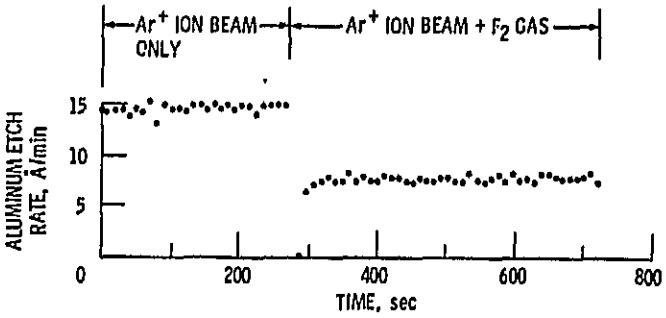

Figure 13. - Ion-assisted gas-surface chemistry using Ar^+ and F_2 on aluminum (involatile reaction product). Ar^+ energy, 450 eV; Ar^+ current, 3.0 μA; F_2 flow, 0 ($t < 270$ sec); and F_2 flow, 2×10^{15} mol/sec ($t > 270$ sec).

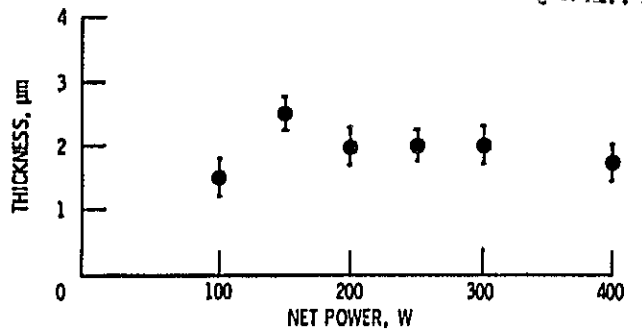

(a) Silicon deposition.

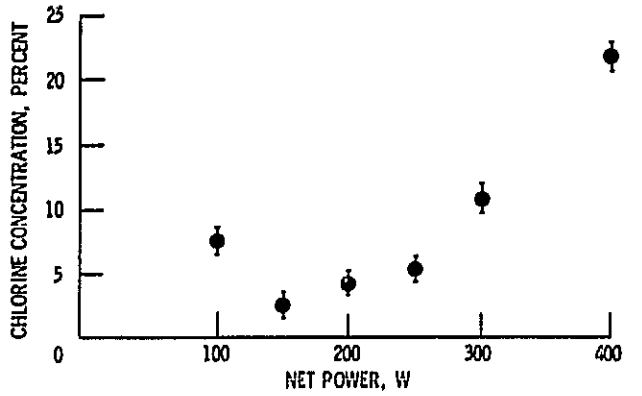

(b) Chlorine contamination.

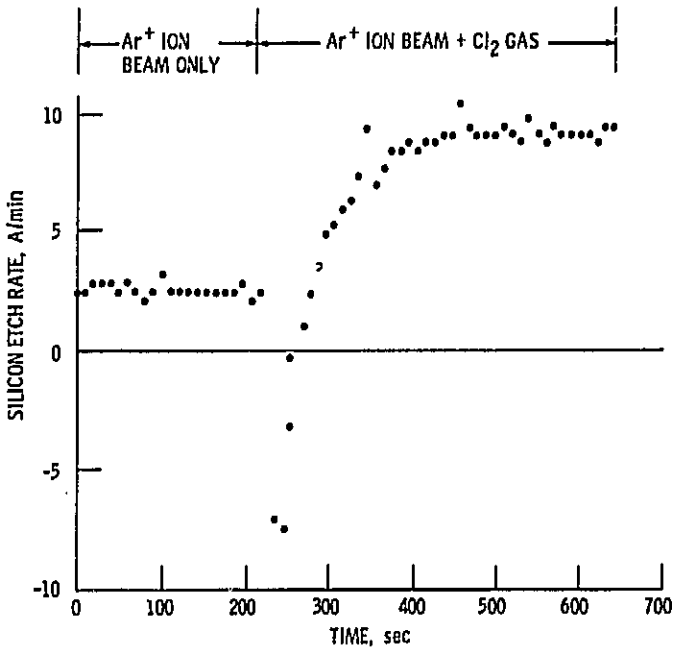

(c) Ion enhanced etching.

Figure 14. - Silicon deposition, chlorine contamination, and its ion enhanced etching.

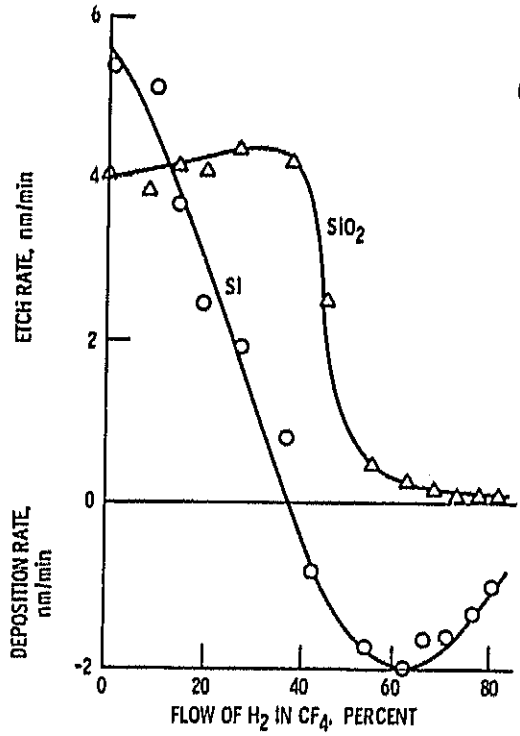

Figure 15. - Deposition and etching rates in a $CF_4 + H_2$ plasma (ref. 14).

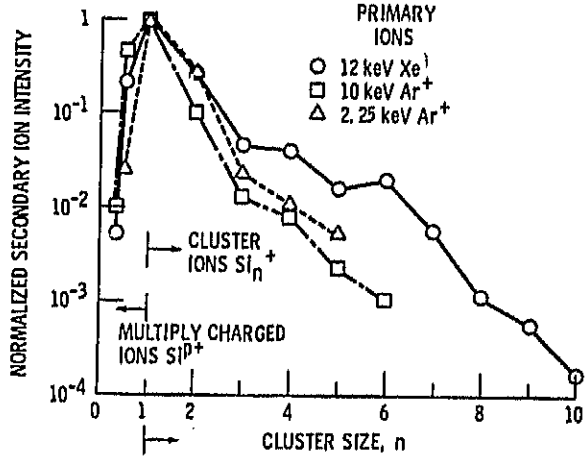

Figure 16. - Silicon clusters sputtered out by Xe^+ and Ar^+ ions (ref. 17).

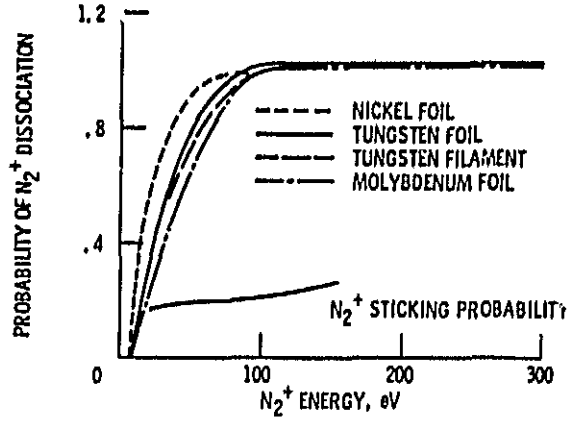

(a) N_2^+ dissociation to N atoms.

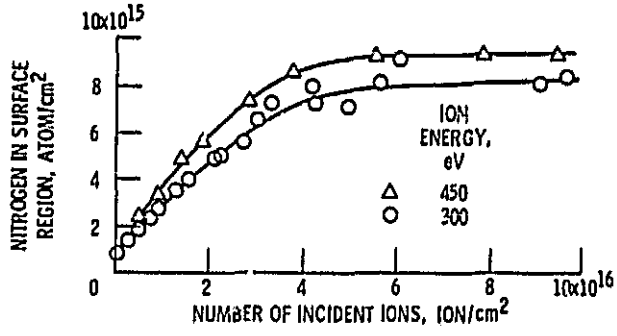

(b) N contained in the surface, WN (30 - 100 A); tungsten.

Figure 17. - Surface chemistry of nitrogen ions (N_2^+) (ref. 15).

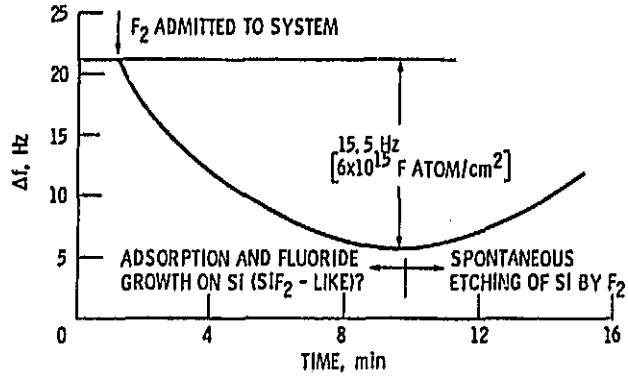

Figure 18. - Surface chemistry of F_2 on silicon (ref. 13).

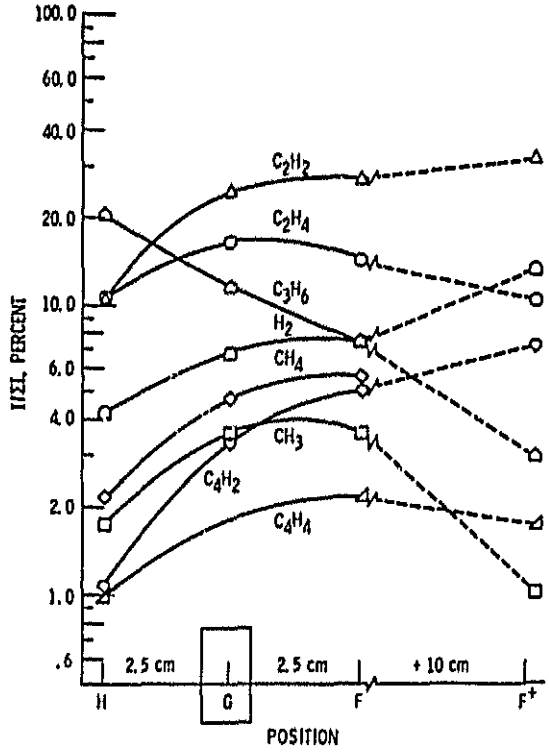

(a) Dissociation of C_3H_6.

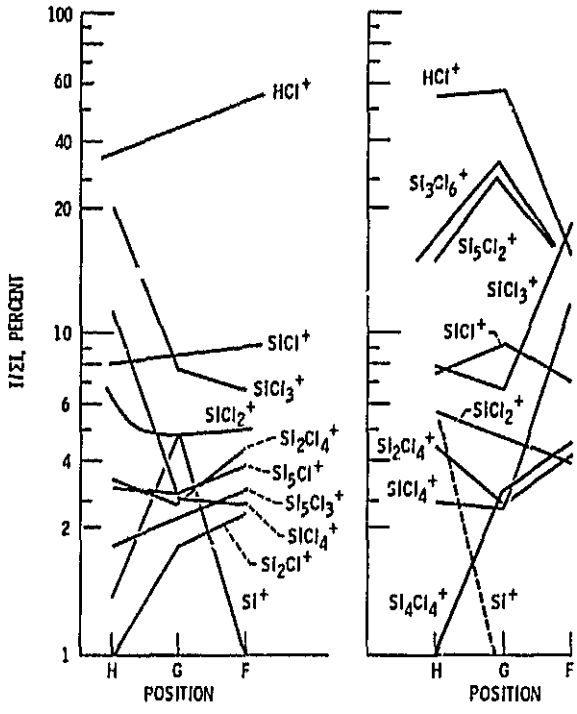

(b) Dissociation of $SiCl_4$.

Figure 19. - Formation of active species from the microwave plasmas of 16 vol % C_3H_6 + Ar and 5 vol % $SiCl_4$ + 20 vol % H_2 + Ar.

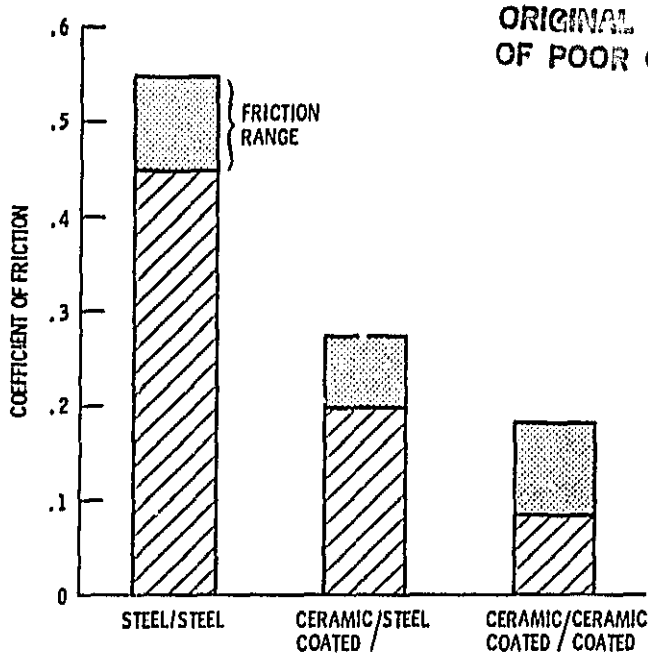

Figure 20. - Coefficient of friction as a function of coated and bare pin and disc combinations during tribotesting. Steels, 440C and 52100; ceramic coatings, carbides and nitrides.

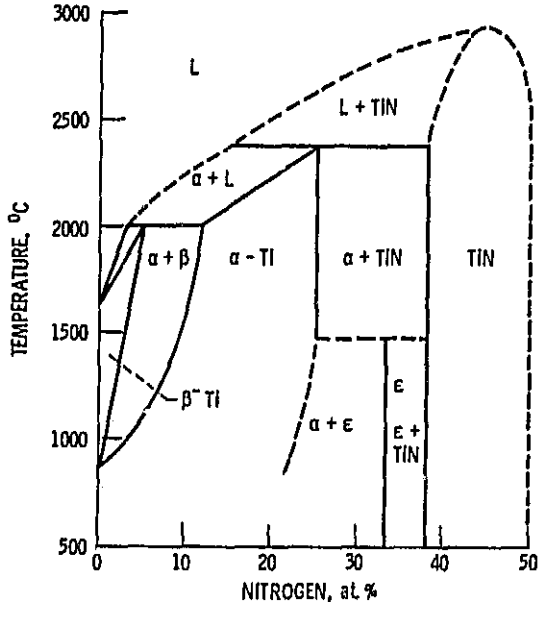

Figure 21. - Proposed phase diagram for titanium-nitrogen.

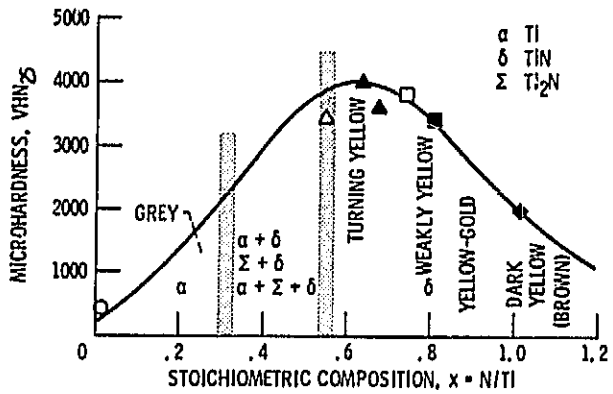

Figure 22. - Microhardness, color and phases of TiN_x as a function of nitrogen stoichiometric composition.